Journal of Asian Ceramic Societies

ISSN: (Print) (Online) Journal homepage: https://www.tandfonline.com/loi/tace20

Designing of porous PMMA/diopside bone cement for non-load bearing applications

Rajan Choudhary, Senthil Kumar Venkatraman, Inna Bulygina, Fedor Senatov, Sergey Kaloshkin & Sasikumar Swamiappan

To cite this article: Rajan Choudhary, Senthil Kumar Venkatraman, Inna Bulygina, Fedor Senatov, Sergey Kaloshkin & Sasikumar Swamiappan (2020) Designing of porous PMMA/diopside bone cement for non-load bearing applications, Journal of Asian Ceramic Societies, 8:3, 862-872, DOI: 10.1080/21870764.2020.1793476

To link to this article: https://doi.org/10.1080/21870764.2020.1793476

Published online: 20 Jul 2020.

JOURNAL OF ASIAN CERAMIC SOCIETIES
2020, VOL. 8, NO. 3, 862–872
https://doi.org/10.1080/21870764.2020.1793476

THE CERAMIC SOCIETY OF JAPAN
THE KOREAN CERAMIC SOCIETY
Taylor & Francis
Taylor & Francis Group

FULL LENGTH ARTICLE

Designing of porous PMMA/diopside bone cement for non-load bearing applications

Rajan Choudhary[a], Senthil Kumar Venkatraman[b], Inna Bulygina[a], Fedor Senatov[a], Sergey Kaloshkin[a] and Sasikumar Swamiappan[b]

[a]Center for Composite Materials, National University of Science and Technology "Misis", Moscow, Russia; [b]Department of Chemistry, School of Advanced Sciences, Vellore Institute of Technology, Vellore, India

ABSTRACT

The objective of the current study was to design a bioactive and mechanically stable ceramic/polymer cement for repairing bone defects. Solvent casting method was utilized to prepare porous diopside/PMMA scaffolds. The characteristic functional groups associated with diopside and PMMA in the composites were confirmed by FT-IR spectroscopy. Scanning electron microscopy revealed that the surface of composites covered by small non-uniform pores having dimensions below 4 µm. It was found that the porosity of the composites can be altered by varying the content of filler (diopside) in the composites. The biomineralization ability and mechanical strength of PMMA were enhanced by fabricating it as a composite with diopside. The presence of apatite peaks on the surface of diopside/PMMA composites was observed after 4 weeks of immersion in SBF solution. The mechanical strength of diopside/PMMA composites was found to match with cancellous bone. Hence, the compositional ratio and constituents played a key role in determining the activity of the composites. Bioactive silicates can be used as a filler in biomedical polymers for imparting ductility to ceramics for achieving advanced functionalities.

ARTICLE HISTORY
Received 6 April 2020
Accepted 28 June 2020

KEYWORDS
Bioceramic; composites; compressive strength; apatite deposition; PMMA

1. Introduction

Diopside belongs to the family of ternary silicate bioceramics with the chemical composition of CaO-MgO-2SiO_2. The cytocompatibility, biodegradability, and apatite deposition ability of diopside have attracted the attention of various research groups to find its application in the field of biomedical engineering [1]. The remarkable *in vitro*/*in vivo* osteogenesis response of diopside makes it as a potential candidate for hard tissue regeneration and periodontal tissue engineering [2,3].

The self-hardening ability and superior mechanical properties of poly(methyl methacrylate) (PMMA) when compared to other synthetic polymers makes it a useful and practical material for fixing implants with bone [4]. PMMA provides immediate structural support to the metallic implant but due to its bioinert nature, it shows negligible chemical and biological interaction with bone. Hence, PMMA is considered as a weak link between implant and bone [5]. Moreover, the inert behavior of PMMA results in osteolysis and loosening of the implant under the influence of repeated interfacial movements (wear debris) [6]. These challenges can be overcome by introducing the bioactive ceramics as a filler in the polymer matrix [7]. This provides adequate osteoconductivity and sufficient mechanical stability to the resultant composite. PMMA reinforced hydroxyapatite shows good anchorage of human osteoblast cells (HOB), enhanced proliferation as well as alkaline phosphatase (ALP) activity [8]. The activity of alkaline phosphatase is considered to indicate the presence of osteoblast cells and the formation of new bone [9]. Renteria-Zamarron et al. (2009) indicated that the PMMA containing 39% of wollastonite exhibits good apatite formation ability and optimum compressive strength [5]. Lee and Rhee (2009) suggested PMMA/SiO_2-CaO nanocomposites as a filler material in dental composite and bone cement [4].

The bone formation and resorption process are regulated by several agents including growth factors, proteins, and hormones [10]. It has been found that different ions, such as phosphorus, calcium, strontium, magnesium, silica, etc., are involved in bone regeneration, mineralization, and metabolism [11]. These therapeutic inorganic ions also act as potential network modifiers for the development of promising bone substituents. Thus, a slight modification in chemical composition alters the structural, chemical, and biological properties of a material.

An earlier study indicated that substitution of silica in HAp resulted in rapid apatite deposition ability and higher cell proliferation, differentiation than pure HAp [12]. Extensive research has been conducted by various groups toward exploring different silicate bioceramics

CONTACT Sasikumar Swamiappan vitsasi@yahoo.co.in

for hard tissue regeneration. Calcium silicate (wollastonite) possesses good biomineralization ability but the faster degradation rate leads to insufficient mechanical strength whereas magnesium silicate (forsterite) has good mechanical stability and poor apatite deposition ability due to their chemical constituents [13,14]. Hence, these limitations can be overcome by exploring ternary calcium magnesium silicate bioceramics having the combined benefits of both calcium silicates and magnesium silicates. Chen et al. (2015) suggested that amongst all calcium magnesium silicates (merwinite, akermanite, and monticellite) diopside was found to have a most stable structure in a physiological environment, noteworthy bioactivity, and highest mechanical strength [15].

Billions of eggshells are discarded as waste by the nutrition and food processing industries. The inadequate disposal of eggshell often causes environmental problems. The abundance and natural origin of the eggshell have attracted the attention of researchers toward their conversion into a valuable product [16]. An eggshell is a protective outer covering of an egg and helps in the exchange of moisture and air (semipermeable membrane). Eggshell powder is considered as an effective calcium supplement as it is composed of approximately 94% calcium carbonate (calcite). Other active compounds include calcium phosphate (1%), magnesium carbonate (1%), and remaining organic matter (4%) [17]. Eggshells are also reported to have health-promoting properties such as bone mineralization and growth, treatment of osteoporosis, and used as a bone graft [18–20]. These characteristics indicate eggshell as a promising raw material for biomedical applications.

Siddharthan et al. (2009) observed inheritance of Na, Mg, Sr, and Si ions in a minor amount from eggshell during the synthesis of nanocrystalline apatite and suggested that these ions can have significant benefits to physiological function [21]. Further, a comparative study between larnite/chitosan composite prepared from eggshell and synthetic calcium nitrate showed rapid biomineralization ability of eggshell-derived composite [22]. Thus, in the current work, a cost-effective and environment-friendly approach for sustainable recycling of waste was adopted to synthesize diopside. Eggshell was utilized as a calcium source to replace expensive synthetic reagent. This practice also satisfies the European societal challenge of conversion of waste into biomaterial for improving the quality of life of bone disease patients.

To the best of author's knowledge, the incorporation of diopside in PMMA matrix has not been reported so far. Thus, the purpose of the current study is to induce biomineralization and improve the mechanical stability of organic cement (PMMA) by incorporating an inorganic bioactive system (diopside ceramic) as a filler for bone cement applications. The influence of chemical constituents and compositional ratio of organic/inorganic components on apatite deposition ability, compressive strength, and Young's modulus was studied.

2. Experimental procedure

2.1. Materials and methods

Glycine (99.5%, AR, SDFCL), Eggshell Powder, Tetraethyl Ortho Silicate (98%, Acros Organics), Magnesium Nitrate (99.0%, LR, SDFCL), Concentrated Nitric Acid (69–72%, LR, SDFCL). PMMA (Avg. molecular weight 15,000, HIMEDIA), Chloroform AR (99.4%, SDFCL), Ethanol AR (99.9%, Changshu Yangyuan Chemicals), Sodium Chloride AR (99.9%, SDFCL), Sodium Bicarbonate AR (99%, SDFCL), Potassium Chloride AR (99.5%, SDFCL), Di-potassium Hydrogen Orthophosphate AR (99.0%, SDFCL), Magnesium Chloride AR (99.0%, SDFCL), Conc. Hydrochloric Acid LR (35–38%, SDFCL), Calcium Chloride AR (98%, SDFCL), Sodium Sulfate Anhydrous AR (99.5%, SDFCL), Tris(hydroxymethyl)aminomethane AR (99.8%, SDFCL) and Deionized water. All the materials were used as such without any further purification.

2.2. Sol-gel combustion synthesis of diopside powders

Diopside powders were synthesized by sol-gel combustion method as per our recent publication [23]. The oxidant (metal nitrate) and organic fuel (glycine) were used in stoichiometric ratio. The oxidant/fuel ratio is calculated as per Equation (1). Thus, glycine was mixed with deionized water to prepare a 2.22 M stock solution.

$$\Phi(\text{glycine}) = \frac{\text{Oxidation valency of calcium and magnesium nitrate}}{-(\text{reducing valency of glycine})} = \frac{-20}{-9} = 2.22\ M \quad (1)$$

Eggshell-derived calcium nitrate solution was utilized as a calcium source for the preparation of diopside. Eggshells were collected from VIT mess and washed under the running tap water to clean their surfaces. The bacterial contamination and unnecessary protein coatings were eliminated by boiling at 120°C for 3 hours with continuous stirring on a magnetic stirrer. The boiled eggshells were transferred to a sheet of tissue paper to absorb water droplets from the surface. Later, the eggshells were dried in a hot air oven at 150°C for a day. The dried eggshells were crushed and grinded manually to fine powders by using agate mortar and pestle. The powdered eggshell was further utilized to prepare a 1 M calcium nitrate solution by adding 37.5 ml

of concentrated nitric acid to 25 gm eggshell powder. A sudden brisk effervescence giving foam-like appearance was noticed due to the liberation of carbon dioxide (CO_2) and water (H_2O). The foamy mixture was kept undisturbed for about 12 hours to facilitate the completion of the reaction. The unreacted content of the solution was separated by filtering through Whatman 41 filter paper. The resultant filtrate was collected in a standard flask and made up to 250 ml by using deionized water. The concentration of calcium ion in the stock solution was estimated by ethylenediaminetetraacetic acid (EDTA) titration by following the procedure mentioned elsewhere [24]. The estimated calcium ion concentration in the eggshell stock solution was observed to be 0.99 molar.

The equimolar concentration of magnesium nitrate and eggshell-derived calcium nitrate were mixed in a beaker and stirred until a homogeneous solution is obtained. Later glycine stock solution was transferred into the beaker containing reaction mixture followed by the addition of tetraethyl orthosilicate (2 M). In order to initiate the hydrolysis of tetraethyl orthosilicate, leading to polycondensation and conversion of solution into gel. The pH of the resultant solution was adjusted to 1.7 by dropwise addition of concentrated nitric acid under constant stirring. The formation of viscous gel-like network was observed in the beaker after stirring for 10 hours and 30 min heating at 50°C. The gel was aged for about a week and then converted into powdered mass by drying in a hot air oven at 150°C. The dried gel was further heated in a muffle furnace at 400°C for half an hour to facilitate the combustion. During this process, an exothermic reaction occurs between glycine (reducing agent) fuel and nitrates (oxidizing agent) leading to the generation of heat and evolution of gasses. The heat assists in the crystallization of product whereas gasses generate porosity in the decomposed product. Finally, the combusted precursor was purified by calcination at 1100°C for 6 hours [23].

2.3. Fabrication of diopside/PMMA composites

The pure diopside was grinded to fine powder and used as a reinforcing filler in the PMMA matrix for fabricating its composites. Figure 1 shows the scheme adopted for preparing diopside/PMMA composites. Solvent casting method was used to prepare diopside/PMMA composites of different compositions as shown in Table 1. The PMMA, supplied as beads, was dissolved in chloroform at a concentration of 20% (w/v). The mixture was stirred until the homogeneous solution of PMMA was achieved. To this solution, a specified amount of finely grinded diopside powder was added and stirred constantly for 2 h in order to ensure the uniform dispersion of diopside powders in the mixture. The resultant mixture of diopside/PMMA/chloroform was heated at 80°C for about 30 min to allow evaporation of chloroform. The slurry obtained was casted in Teflon mold to prepare cylindrical scaffolds (13 mm × 6.5 mm) and air-dried for overnight in a fume hood. Finally, the samples were vacuum dried to remove the chloroform vapors trapped inside the voids. The composites were washed with deionized water followed by ethanol and stored in a dried vacuum desiccator until further use. A similar procedure was followed for the preparation of pure PMMA scaffold without diopside.

2.4. In vitro experiments

2.4.1. Preparation of SBF

The SBF was prepared in a single batch by dissolving the chemicals of the analytical grade in the sequence as per Kokubo and Takadama protocol [25]. The appropriate quantities of reagents for the preparation of SBF were dissolved sequentially in 1 liter double-distilled water with constant stirring at room temperature. The pH of the SBF was adjusted to 7.4 ± 0.2 by dropwise addition of 1 M HCl and the prepared SBF was stored in the refrigerator.

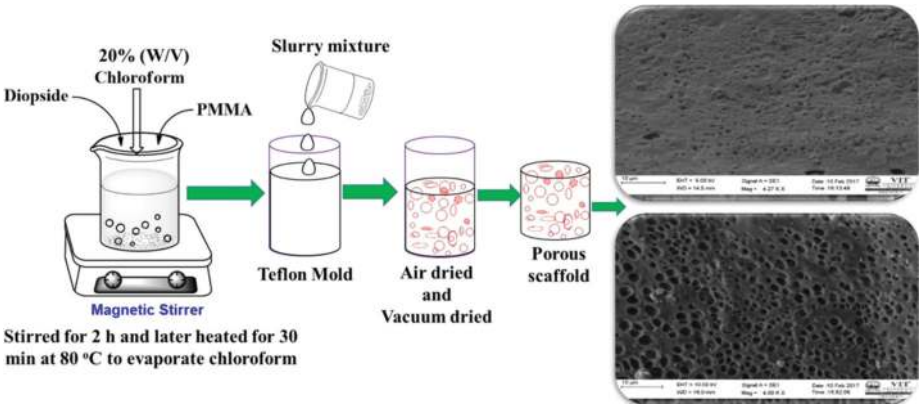

Figure 1. Scheme utilized for preparing diopside/PMMA composites.

Table 1. Composition of diopside/PMMA composites.

S. No	Code	Composition of diopside (wt %)	Composition of PMMA (wt %)
1	DP1	75	25
2	DP2	50	50
3	DP3	25	75

2.4.2. Biomineralization assay

The apatite deposition ability of diopside/PMMA composites was studied by immersing it in SBF. The samples were placed separately in conical flasks containing SBF solution (50 mL) and incubated under a non-shaking condition at 37°C ± 0.3. The SBF solution was changed after every 24 h in order to provide a constant supply of essential ions responsible for apatite precipitation. After 14th and 28th day, the samples were removed from the SBF, washed with double-distilled water, and dried at room temperature prior to the surface analysis by XRD and SEM/EDX.

2.4.3. Mechanical testing

Vadgama (2005) stated that an ideal scaffold should offer sufficient structural support to the regenerating tissues during degradation and remodeling [26]. Therefore, the diopside/PMMA composites were planned to immerse in refreshed SBF and after 1 month their mechanical behavior was compared with the mechanical properties of the bone (cancellous, cortical). The procedure followed for the preparation of diopside/PMMA composites for mechanical studies was carried out as per ASTM specifications (13 mm diameter and 6.5 mm height) [15]. The diopside/PMMA composites were immersed in SBF maintained at 37°C ± 0.3. After 30 days, the composites were taken out from SBF, washed with deionized water, and dried for 1 day at room temperature. The dried samples were examined for mechanical stability by using the UTM INSTRON 8801 with a load weight accuracy of ± 0.5%. The composites were tested at an extension rate of 1.5 mm (pure PMMA, DP2, and DP3) and 0.8 mm (DP1) at a compression rate of 1 mm/min. The test was repeated three times for each composite and the data were given as a mean with the standard deviation.

3. Characterization

Powder X-Ray Diffractometer (Bruker, D8 advance, Germany), using Cu Kα, Ni-filtered radiation was used for phase identification of the composites. The maximum angular accuracy allowed for 2θ deviation was ± 0.010. Functional groups present in the composites were confirmed by FT-IR spectroscopy (IR Affinity-1, Shimadzu FT-IR spectrophotometer). The FT-IR spectrum was recorded from 4000 to 400 cm^{-1} region with 4 cm^{-1} resolution. Scanning electron microscopy (SEM-CARL ZEISS) was used to analyze the surface morphology and energy-dispersive X-ray spectroscopy (EDX-OXFORD Inc.) was used to study the elemental composition of diopside/PMMA composites.

4. Results and discussion

4.1. FT-IR analysis of as-prepared diopside/PMMA composites

The characteristic functional groups associated with diopside and PMMA in the composites were confirmed by FT-IR spectroscopy (Figure 2). The bending vibrations of diopside were noticed at 412 cm^{-1} (O-Ca-O), 464–509 cm^{-1} (O-Mg-O), and 634–675 cm^{-1} (O-Si-O) while stretching vibrations were observed at 840–983 cm^{-1} (Si-O) and 1064 (Si-O-Si) respectively [27]. These observed data were found similar to recently published reports and confirmed the presence of diopside in the composites. Duan et al. (2008) studied the IR spectra of PMMA and observed all the essential vibrational bands associated with it [28]. The doublet at 2951–2995 cm^{-1} was assigned to C-H stretching vibrations while the bending vibration of C-H group was noticed at 1437 cm^{-1}. The sharp peak at 1722 cm^{-1} reveals the presence of acrylate carboxyl group. The C-O-C stretching vibration was detected in the range of 1143–1271 cm^{-1}. The dual α-methyl bands were found at 748 and 1373 cm^{-1}.

4.2. XRD analysis of as-prepared diopside/PMMA composites

Figure 3 shows the XRD pattern of the as-prepared diopside/PMMA composites. Figure 3(a) shows an intense peak at 22.49° corresponding to PMMA as per the earlier report [29]. The XRD pattern shown in Figure 3(b) reveals the existence of all characteristic peaks associated with pure crystalline diopside. XRD pattern of DP1 composite (Figure 3(c)) shows diopside as primary phase along with PMMA as a secondary phase. The high intensity of diopside peaks is due to the higher concentration of diopside in the composite. In the case of DP2 composite (Figure 3(d)), an amorphous background was detected comprising dual phases including diopside and PMMA.

The PMMA emerged as a major phase (Figure 3(e)) as its quantity is high (75%) in DP3 composite. This causes a reduction in the intensity of diopside peaks and the pattern shows an amorphous characteristic due to the presence of polymer content.

4.3. Surface morphology analysis of diopside/PMMA composites

The surface topography such as porosity, morphology, surface area of scaffold plays a key role in tissue regeneration. Literature survey suggested that the presence of porous network assists in promoting cell migration,

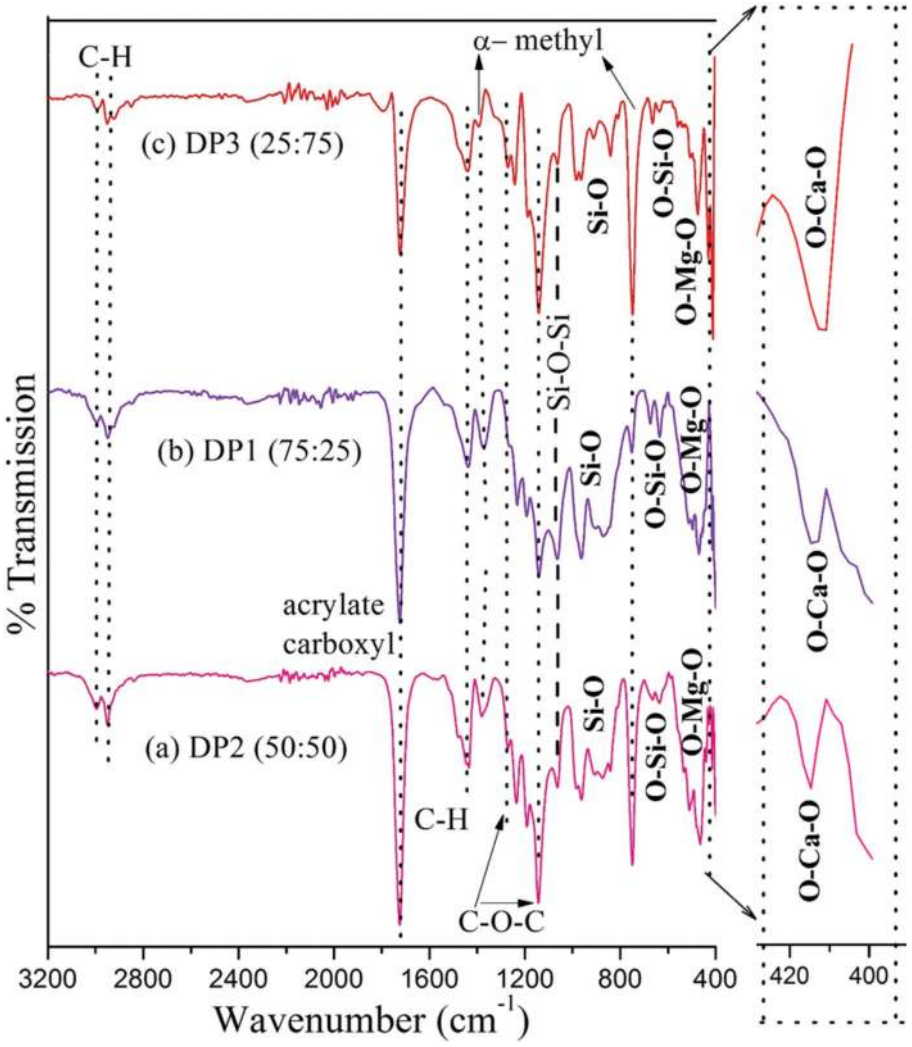

Figure 2. FT-IR spectra of as-prepared diopside/PMMA composites.

vascularization, tissue ingrowth, nutrient delivery to the regenerating tissue, and also facilitates the removal of metabolic products [30]. Moreover, the optimal porosity of a scaffold is also dependent on the type of tissue.

The surface morphology of the composites was studied by scanning electron microscopy. The composites reveal different topography with the presence of small pores spread on its surface (Figure 4). The evolution of chloroform during drying resulted in the formation of non-uniform pores over the surface of DP1 composite (Figure 4(a)). As the composition of diopside was reduced to 50%, an increment in the porosity (average pore size of 0.93 μm) was observed (Figure 4(b)). This indicates that the porosity of the composites can be altered by varying the content of filler (diopside) in the composites. The DP3 composite shows honeycomb-like morphology and the surface was entirely covered by pores of 2 μm dimensions (Figure 4(c)). The surface of pure PMMA (Figure 4(d)) was found to have numerous elongated structures of different shapes. The average size of the pores was observed as 45 μm.

4.4. Elemental analysis of diopside/PMMA composites

The elemental analysis of composites shows characteristic peaks associated with both diopside (Ca, Mg, Si, O) and PMMA (C, O) which confirms their chemical composition (Figure 5(a–c)). The EDX spectra of pure PMMA (Figure 5(d)) shows the presence of intense peaks corresponding to carbon (C) and oxygen (O) which satisfies the chemical formula of PMMA.

4.5. Biomineralization studies

4.5.1. XRD analysis of deposited apatite

The diopside/PMMA composites were immersed in the SBF to study their apatite deposition ability (Figure 6). The composites were found to be inactive even after 14 days as no apatite deposition was observed on their surface (Figure 6(b, e)). An amorphous phase was detected on the surface of DP1 and DP2 composites after 28 days along with an emerging apatite peak (Figure 6(c, f)). Liu et al. (2015) observed an increase in apatite deposition with the increase in mesoporous

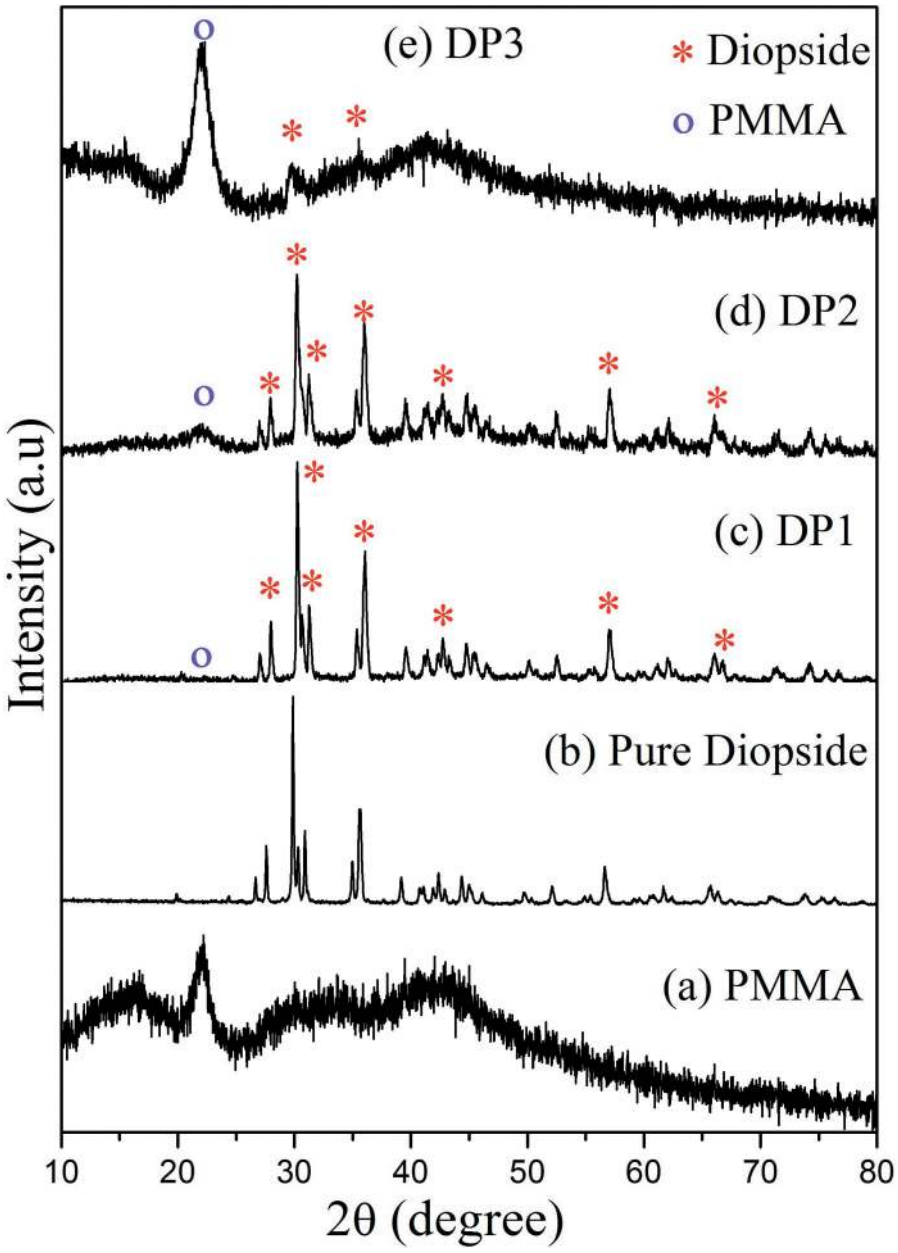

Figure 3. XRD patterns of as-prepared diopside/PMMA composites.

diopside content in poly-L-lactic acid (PLLA) matrix [31]. The composites composed of 40% diopside show better apatite deposition than 20%. Hence, DP1 and DP2 composites indicate a content-dependent response toward apatite deposition.

4.5.2. Surface morphology and elemental analysis of deposited apatite

The surface of DP1 and DP2 composites after 4 weeks of immersion in the SBF medium was characterized by scanning electron microscopy (Figure 7). The surface of DP1 composite was uniformly covered by mesh-like interconnected structures having fibrous morphology (Figure 7(a, b)). DP2 sample shows the presence of aggregated particles deposited over its surface (Figure 7(d, e)). The presence of phosphorus along with calcium, magnesium, silicon, and oxygen in the EDX pattern indicates the deposition of apatite phase over the surface of composites (Figure 7(c, f)).

The Ca/P atomic ratio of DP1 composite was noticed as 1.34 whereas in the case of DP2 it was 1.69. Yubao et al. (1994) emphasized that apatite with a common formula $Ca_{10-x}(HPO_4)_x(PO_4)_{6-x}(OH)_{2-x}$ ($0 < x < 2$) is known as non-stoichiometric or calcium-deficient apatite and the Ca/P ratio ranges between 1.33 and 1.67 [32]. Moreover, Dorozhkin (2010) stated that the Ca/P ratio ranging from 1.22 to 2.2 corresponds to amorphous calcium phosphate [33]. This can be correlated with the appearance of amorphous background detected in XRD patterns (Figure 6) after immersion in SBF. Based upon these observations, it can be indicated that the surface of DP1 and DP2 composites was composed of amorphous Ca-P phase.

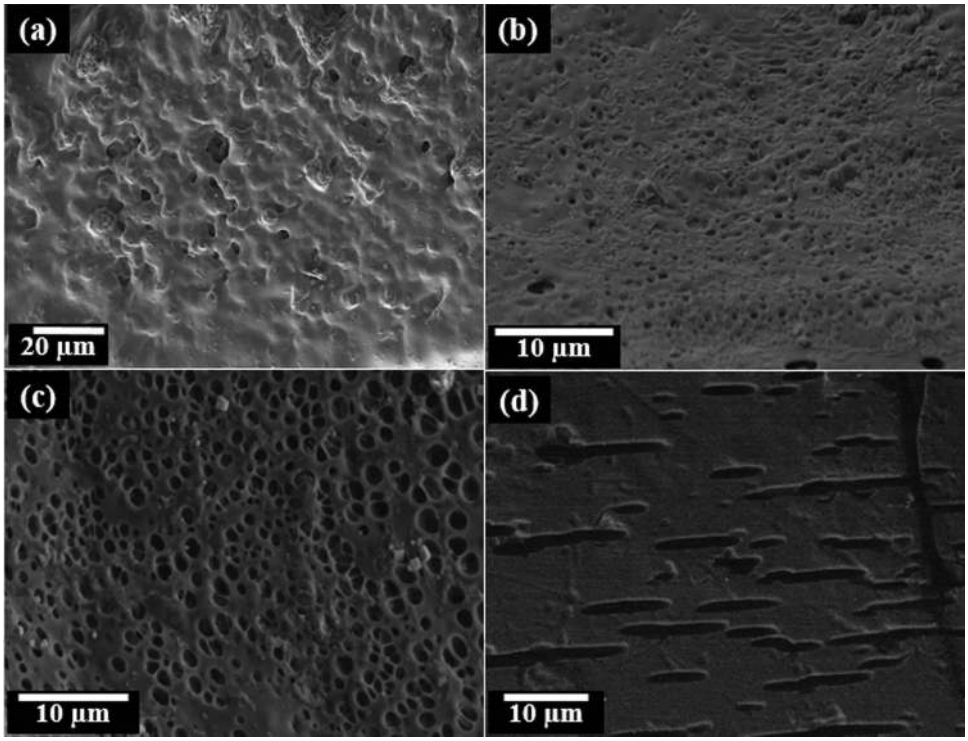

Figure 4. SEM Micrographs of DP1 (a), DP2 (b), DP3 (c), and PMMA (d).

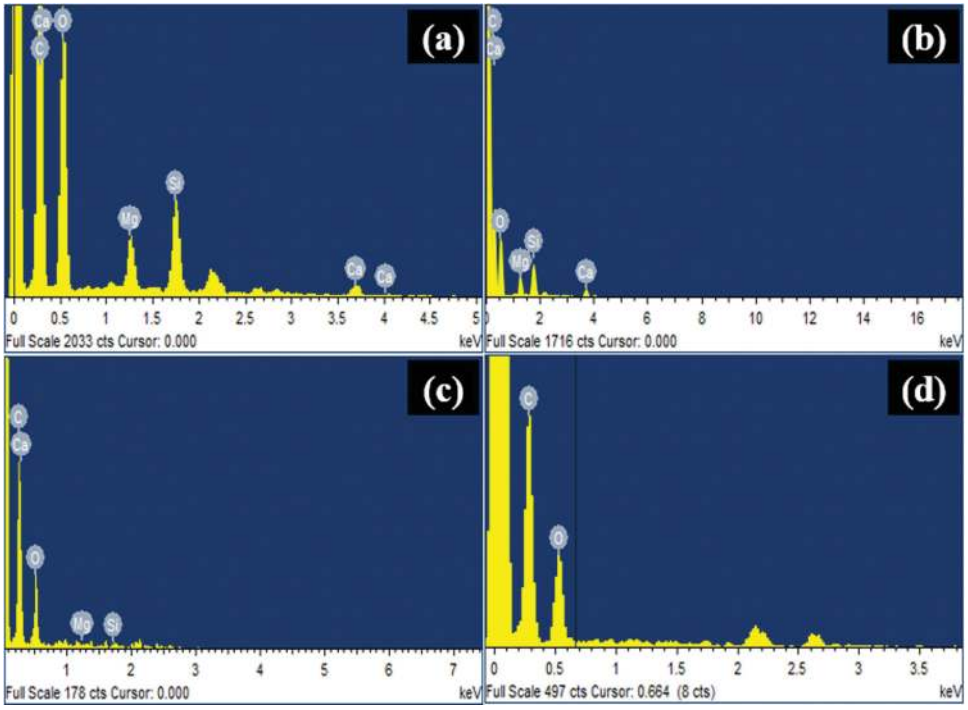

Figure 5. EDX Spectra of DP1 (a), DP2 (b), DP3 (c), and PMMA (d).

The mechanism involved in the biomineralization activity at the composite/SBF interface can be explained as: Initially, alkali earth cations from the sample (Ca^{2+}, Mg^{2+}) are exchanged with H^{+} anions present in the SBF. This leads to the breakdown of the silica network and formation of silanol (Si-OH) at the interface. This silanol further reacts with OH^{-} ion to form a silica-rich layer ($Si\text{-}O^{-}$) at the interface followed by the liberation of water. This negative charge at first attracts cations (Ca^{2+}, Mg^{2+}) and later anions (PO_4^{3-}) from the SBF resulting in the formation of an amorphous calcium phosphate layer. Finally, the CO_3^{2-} and OH^{-} anions present in the SBF crystallize the amorphous Ca-P layer into calcium deficient hydroxycarbonate apatite (HCA) [34]. The transformation of amorphous calcium phosphate into stable apatite is found to be influenced by the presence of magnesium ion [35]. Thus, the crystallization of amorphous calcium

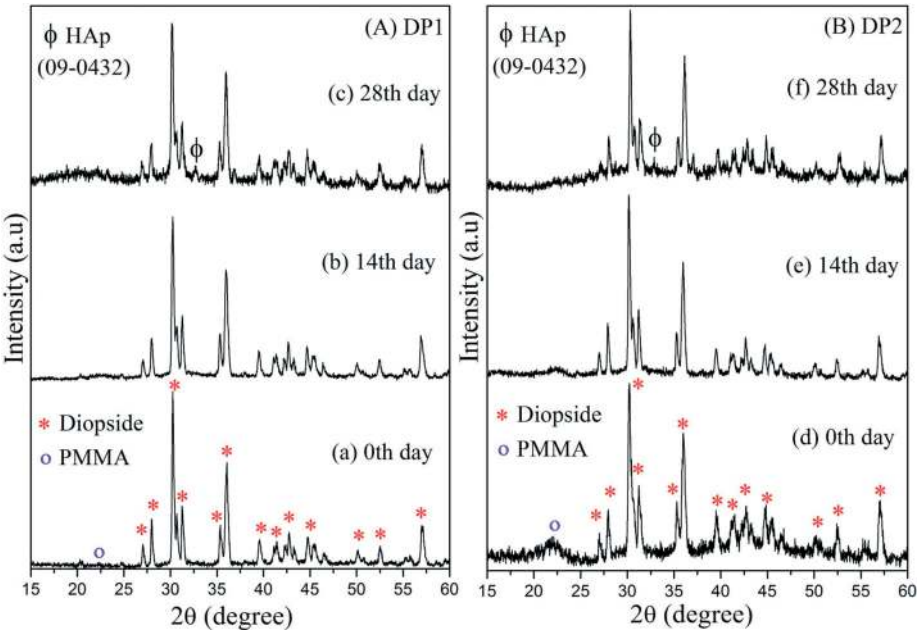

Figure 6. XRD patterns of diopside/PMMA composites after immersion in SBF.

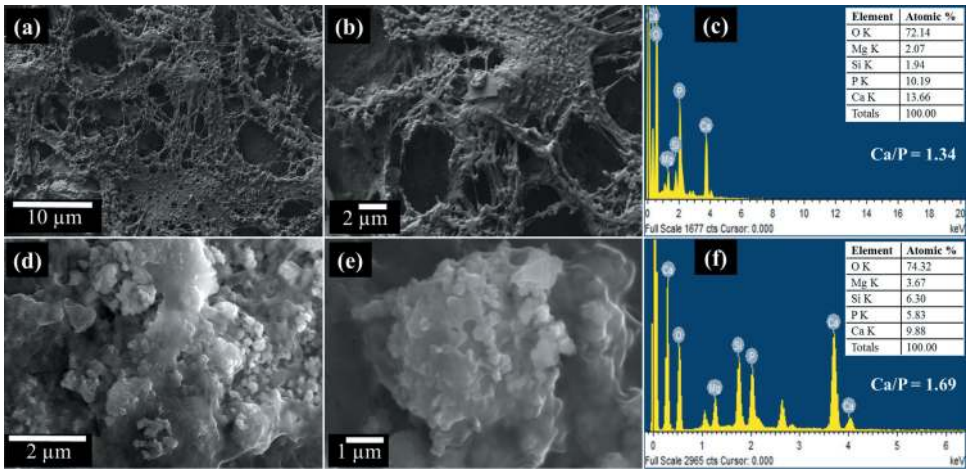

Figure 7. SEM/EDX micrographs of DP1 (a, b, c) and DP2 (d, e, f) composite after immersion in SBF.

phosphate was delayed and its presence was noticed even after 4 weeks of immersion.

4.6. Mechanical studies of composites after immersion in SBF

The diopside/PMMA composites behaved differently under the influence of external mechanical force as shown in Figure 8. The DP1 composite experienced brittle failure and broke down into smaller fragments. This was due to the brittle nature of the ceramic that has dominated in the composite as DP1 sample contains about 75% of diopside. The DP2 sample shows ductile failure during mechanical testing, as the composite contains an equal concentration (50%) of ceramic and polymer. Hence, the failure point was balanced by both phases. In the case of DP3 composite, minor cracking was observed and change in the dimensions of the sample was noticed. In other words, the DP3 composite experienced structural deformation resulting in a change in their geometry. Thus, the samples were bulged out to form an oval shape under the influence of an external mechanical stress. This may be due to the highly flexible nature of the polymer.

Diopside/PMMA composite with 50:50 ratio possesses the highest compressive strength of 10 MPa and Young's modulus of 120 MPa. Increase in the amount of diopside in DP1 composite causes a reduction in mechanical properties (compressive strength 6 MPa and Young's modulus 90 MPa). When the polymer ratio was increased in DP3 composite, the compressive strength and Young's modulus of the scaffolds decrease to 4 MPa and 40 MPa, respectively. Pure PMMA exhibits inferior mechanical stability (compressive strength: 2 MPa, Young's modulus: 30 MPa) when compared to the composites. This analysis shows that the presence of diopside as filler in polymer matrix

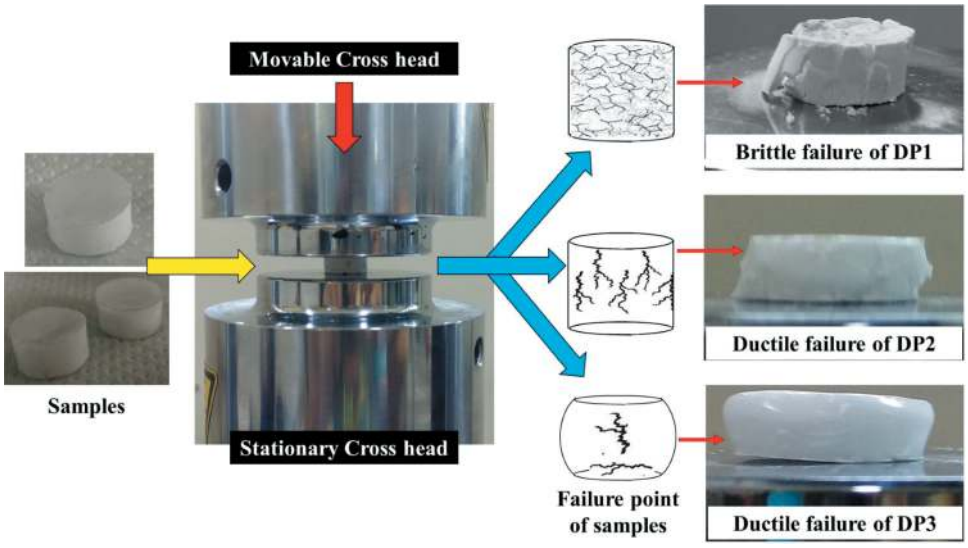

Figure 8. Mechanical behavior of diopside/PMMA composites.

enhanced the mechanical properties of the composite. It was also observed that increasing the diopside content in the composites leads to a decrease in their mechanical properties. An earlier report suggested that a critical concentration exists for each material beyond which the addition of filler reduces the mechanical properties of the composites [36].

The maximum mechanical properties of DP2 composite can be explained based upon chemical constituents. DP2 contains an equal amount of PMMA and diopside content. As a result, the mechanical stress was balanced by both the materials leading to ductile failure. He et al. (2016) emphasized the influence of apatite deposition on the mechanical strength of the material [37]. It was reported that during biomineralization, the apatite (Ca-P) fills the pores and increases the strength of the scaffold. Thus, the Ca/P ratio of DP2 composite after immersion in SBF was found to be 1.69 which indicated that the biomineralization over the surface of DP2 composite was more rapid. That is why the mechanical properties of the DP2 composite were enhanced. From the above discussion, it is clear that among all composites, DP2 has the potential to withstand more mechanical load and possess good apatite deposition ability.

Chen et al. (2015) investigated the mechanical behavior of diopside/PCL composites and reported the maximum compressive strength of 0.3 MPa and Young's modulus of 13 MPa [15]. Wei et al. (2008) observed that the compressive strength and Young's modulus values of calcium silicate/PCL composites got reduced when the content of calcium silicate was increased to 60% [36]. The composites with 40% calcium silicate content showed superior mechanical strength than 60%.

A comparison between mechanical properties of diopside/PMMA composites and natural bone [34] is shown in Table 2. All diopside/PMMA composites and pure PMMA fall in between the lower and upper limit of the compressive strength of cancellous bone. Similarly, the values of diopside/PMMA composites were noticed to achieve only the lower limit of Young's modulus of cancellous bone. Neither composites nor pure PMMA matched the compressive strength and Young's modulus of cortical bone.

Table 2. Comparative study between mechanical properties of bone 34 and diopside/PMMA composites.

		Mechanical properties	
Samples		Compressive strength (MPa)	Young's modulus (MPa)
Cancellous Bone [34]		0.1–16	50–500
Cortical Bone [34]		130–200	7000–30,000
Diopside/PMMA composites	DP1	6 ± 1.2	90 ± 0.1
	DP2	10 ± 1.7	120 ± 0.0
	DP3	4 ± 1.4	40 ± 0.0
Pure PMMA		2 ± 0.6	30 ± 0.0

Diopside/PMMA composites possess good mechanical stability concerning cancellous bone even after 1 month of immersion in SBF. This suggests that the composites can provide adequate structural support to the regenerating tissues during the remodeling process. Thus, the current study presents a beneficial approach for predicting the mechanical behavior of samples. This report proposes that these composites can be either utilized for healing the defected sites of cancellous bone or repairing soft tissues where mechanical stress is not a primary criterion.

5. Conclusion

Porous diopside/PMMA composites were prepared by the solvent casting method. The current report indicated that the addition of the diopside as a filler into the PMMA matrix has enhanced the mechanical properties as well as induced apatite deposition over the surface of composites within 4 weeks of immersion. The composites

revealed a content-dependent response toward biomineralization and mechanical stability. The compressive strength and Young's modulus of composites were matched with the lower limits of the cancellous bone. The surface of composites after immersion in SBF was covered by interconnected mesh-like structures. Amongst all formulations, the composites containing 50% diopside have shown good apatite deposition ability and appropriate mechanical strength. The present study concludes that appropriate control over chemical constituents and compositional ratios can assist in designing potential scaffolds for biomedical applications.

Acknowledgments

The authors acknowledge the CAMPT-VIT for helping with the mechanical studies. The authors also thank DST-FIST for the XRD and SEM-EDX characterization. .

Disclosure statement

No potential conflict of interest was reported by the authors.

Funding

This work was supported by the Ministry of Science and Higher Education of the Russian Federation in the framework of Increase Competitiveness Program of NUST «MISiS» (№ K4-2019-018), implemented by a governmental decree dated 16th of March 2013, N 211.

References

[1] Diba M, Goudouri O-M, Tapia F, et al. Magnesium-containing bioactive polycrystalline silicate-based ceramics and glass-ceramics for biomedical applications. Curr Opin Solid State Mater Sci. 2014;18:147–167.
[2] Zhang YF, Li S, Wu CT. The in vitro and in vivo cementogenesis of $CaMgSi_2O_6$ bioceramic scaffolds. J Biomed Mater Res Part A. 2014;102:105–116.
[3] Wu C, Ramaswamy Y, Zreiqat H. Porous diopside ($CaMgSi_2O_6$) scaffold: a promising bioactive material for bone tissue engineering. Acta Biomater. 2010;6:2237–2245.
[4] Lee K-H, Rhee S-H. The mechanical properties and bioactivity of poly(methyl methacrylate)/SiO_2–CaO Nanocomposite. Biomaterials. 2009;30:3444–3449.
[5] Renteria-Zamarron D, Cortes-Hernandez DA, Bretado-Aragon L, et al. Mechanical properties and apatite-forming ability of PMMA bone cements. Mater Des. 2009;30:3318–3324.
[6] Goodman S. Wear particulate and osteolysis. Orthop Clin N Am. 2005;36:41–48.
[7] Shinzato S, Kobayashi M, Mousa WF, et al. Bioactive polymethyl methacrylate-based bone cement: comparison of glass beads, apatite- and wollastonite-containing glass-ceramic, and hydroxyapatite fillers on mechanical and biological properties. Biomed Mater Res Part A. 2000;51:258–272.
[8] Dalby MJ, Di Silvio L, Harper EJ, et al. In vitro evaluation of a new polymethylmethacrylate cement reinforced with hydroxyapatite. J Mater Sci. 1999;10:793–796.
[9] Kuru L, Griffiths GS, Petrie A, et al. Alkaline phosphatase activity is upregulated in regenerating human periodontal cells. J Periodontal Res. 1999;34:123–127.
[10] Murphy S, Wren AW, Towler MR, et al. The effect of ionic dissolution products of Ca-Sr-Na-Zn-Si bioactive glass on in vitro cytocompatibility. J Mater Sci Mater Med. 2010;21:2827–2834.
[11] Hoppe A, Mourino V, Boccaccini AR. Therapeutic inorganic ions in bioactive glasses to enhance bone formation and beyond. Biomater Sci. 2013;1:254–256.
[12] Vallet-Regi M, Arcos D. Silicon substituted hydroxyapatites: a method to upgrade calcium phosphate based implants. J Mater Chem. 2005;15:1509–1516.
[13] Lin KL, Zhai WY, Chang J, et al. Study of mechanical property and in vitro biocompatibility of $CaSiO_3$ ceramics. Ceram Int. 2005;31:323–326.
[14] Kharaziha M, Fathi MH. Improvement of mechanical properties and biocompatibility of forsterite bioceramic addressed to bone tissue engineering materials. J Mech Behav Biomed Mater. 2010;3:530–537.
[15] Chen C, Watkins-Curry P, Smoak M, et al. Targeting calcium magnesium silicates for polycaprolactone/ceramic composite scaffolds. ACS Biomater Sci Eng. 2015;1:94–102.
[16] Choudhary R, Vecstaudza J, Krishnamurithy G, et al. In-vitro bioactivity, biocompatibility and dissolution studies of diopside prepared from biowaste by using sol–gel combustion method. Mater Sci Eng C. 2016;68:89–100.
[17] Ho W-F, Hsu H-C, Hsu S-K, et al. Calcium phosphate bioceramics synthesized from eggshell powders through a solid state reaction. Ceram Int. 2013;39:6467–6473.
[18] Omi N, Ezawa I. Effect of eggshell Ca on preventing of bone loss after ovariectomy. J Home Econ Jpn. 1998;49:277–282.
[19] Rovensky J, Stancikova M, Masarik P, et al. Eggshell calcium in the prevention and treatment of osteoporosis. Int J Clin Pharmacol Res. 2003;23:83–92.
[20] Park JW, Bae SR, Suh JY, et al. Evaluation of bone healing with eggshell-derived bone graft substitutes in rat calvaria: a pilot study. J Biomed Mater Res A. 2008;87:203–214.
[21] Siddharthan A, Sampath Kumar TS, Seshadri SK. Synthesis and characterization of nanocrystalline apatites from eggshells at different Ca/P ratios. Biomed Mater. 2009;4:045010.
[22] Choudhary R, Koppala S, Srivastava A, et al. In-vitro bioactivity of nanocrystalline and bulk larnite/chitosan composites: comparative study. J Sol-Gel Sci Technol. 2015;74:631–640.
[23] Choudhary R, Venkatraman SK, Chatterjee A, et al. Biomineralization, antibacterial activity and mechanical properties of biowaste derived diopside nanopowders. Adv Powder Technol. 2019;30:1950–1964.
[24] Anjaneyulu U, Sasikumar S. Bioactive nanocrystalline wollastonite synthesized by sol–gel combustion method by using eggshell waste as calcium source. Bull Mater Sci. 2014;37:207–212.
[25] Kokubo T, Takadama H. How useful is SBF in predicting in vivo bone bioactivity? Biomaterials. 2006;27:2907–2915.

[26] Vadgama P. Surfaces and interfaces for biomaterials. England: Woodhead publishing limited; 2005.
[27] Najafinezhad A, Abdellahi M, Ghayour H, et al. A comparative study on the synthesis mechanism, bioactivity and mechanical properties of three silicate bioceramics. Mater Sci Eng C. 2017;72:259–267.
[28] Duan G, Zhang C, Li A, et al. Preparation and characterization of mesoporous zirconia made by using a poly (methyl methacrylate) template. Nanoscale Res Lett. 2008;3:118–122.
[29] Devikala S, Kamaraj P, Arthanareeswari M. Sensing of acetone vapours using polymer composite. Orient J Chem. 2016;32:2269–2274.
[30] Liliana P-C, Magda L-E, Jaime ER-V. Scaffold design for bone regeneration. J Nanosci Nanotechnol. 2014;14:15–56.
[31] Liu Z, Ji J, Tang S, et al. Biocompatibility, degradability, bioactivity and osteogenesis of mesoporous/macroporous scaffolds of mesoporous diopside/poly(L-lactide) composite. J R Soc Interface. 2015;12:20150507.
[32] Yubao L, Klein CPAT, JDe W, et al. Shape change and phase transition of needle-like non-stoichiometric apatite crystals. J Mater Sci Mater Med. 1994;5:263–268.
[33] Dorozhkin SV. Bioceramics of calcium orthophosphates. Biomaterials. 2010;31:1465–1485.
[34] Gerhardt L-C, Boccaccini AR. Bioactive glass and glass-ceramic scaffolds for bone tissue engineering. Materials. 2010;3:3867–3910.
[35] Vallet-Regi M, Salinas AJ, Roman J, et al. Effect of magnesium content on the in vitro bioactivity of CaO-MgO-SiO_2-P_2O_5 sol-gel glasses. J Mater Chem. 1999;9:515–518.
[36] Wei J, Heo SJ, Kim DH, et al. Comparison of physical, chemical and cellular responses to nano- and micro-sized calcium silicate/poly(ε-caprolactone) bioactive composites. J R Soc Interface. 2008;5:617–630.
[37] He D, Zhuang C, Xu S, et al. 3D printing of Mg-substituted wollastonite reinforcing diopside porous bioceramics with enhanced mechanical and biological performances. Bioact Mater. 2016;1:85–92.